Net baryon number probability distribution near the chiral phase transition

Kenji Morita,[1,*] Vladimir Skokov,[2] Bengt Friman,[3] and Krzysztof Redlich[4,5]

[1] *Yukawa Institute for Theoretical Physics, Kyoto University, Kyoto 606-8502, Japan*
[2] *Physics Department, Brookhaven National Laboratory, Upton, NY 11973, USA*
[3] *GSI, Helmholzzentrum für Schwerionenforschung, Planckstr. 1, D-64291 Darmstadt, Germany*
[4] *Institute of Theoretical Physics, University of Wroclaw, PL-50204 Wrocław, Poland*
[5] *Extreme Matter Institute EMMI, GSI, Planckstr. 1, D-64291 Darmstadt, Germany*

(Dated: November 21, 2012)

We discuss the properties of the net baryon number probability distribution near the chiral phase transition. Our studies are performed within Landau theory, where the coefficients of the polynomial potential are parameterized so as to reproduce the mean-field and $O(4)$ scaling behaviors of the cumulants of the net baryon number. Within this model, we obtain the probability distribution for the net baryon number in a finite volume and study the effect of critical fluctuations on their properties. We show that in a mean-field approach, the singular part of the probability distribution can be obtained exactly and that it tends to broaden the distribution. By contrast, in the model with $O(4)$ scaling, the contribution of the singular part results in a narrowing of the net baryon number distribution. As expected, we find that the critical structures observed in the cumulants on the $O(4)$ critical line reflect modifications mainly in the tails of the distribution. We explore various methods for computing the probability distributions.

PACS numbers: 25.75.Nq, 24.60.-k, 05.70.Jk

I. INTRODUCTION

Fluctuations of conserved charges reflect the critical properties of a system. In particular, in a strongly interacting medium, fluctuations of the net baryon number and of the electric charge are valuable probes of the QCD phase transition [1–6]. Such fluctuations may provide a signature for the conjectured chiral critical point [7–9], as well as for the residual criticality of the underlying $O(4)$ transition [4, 5, 10–14], expected in QCD at small densities in the limit of massless u and d quarks [15, 16].

Since fluctuations of conserved charges are experimentally accessible, they have been suggested as probes of the proximity of the chiral crossover to the freeze-out line in heavy-ion collisions [5, 10, 17]. A particular role has been attributed to higher order cumulants, which exhibit an enhanced signature for criticality with increasing order [4, 10, 12, 13]. In particular, the sixth- and higher-order cumulants of the net baryon number and of the electric charge vary rapidly in the transition region and even change sign close to the chiral crossover, already at vanishing baryon chemical potential [5, 10, 13, 17].

Consequently, data on charge fluctuations in heavy-ion collisions at LHC and RHIC energies, may provide experimental evidence for the chiral transition of QCD [5, 18]. First measurements of fluctuations of the net baryon number, more precisely the net proton number, in heavy-ion collisions at RHIC have been obtained by the STAR Collaboration [19]. The data are, at least on a qualitative level, consistent with residual criticality, owing to the underlying chiral phase transition.

*Electronic address: kmorita@yukawa.kyoto-u.ac.jp

Cumulants of conserved charges have also been studied theoretically. At small chemical potential $\mu/T \ll 1$, they have been computed in first principle calculations, using lattice QCD [20–23], while at large μ, their properties were explored within effective chiral models [11–13, 24–27], which share the global symmetries of QCD.

In statistical physics, the n-th order cumulant $c_n(T,\mu)$ of a conserved charge N is obtained by differentiating the thermodynamic pressure $p(T,\mu)$ with respect to the corresponding chemical potential μ,

$$c_n(T,\mu) \equiv \frac{\partial^n [p(T,\mu)/T^4]}{\partial(\mu/T)^n}\,. \tag{1}$$

The pressure is related to the grand canonical partition function through $p = (T/V)\ln\mathcal{Z}$. The cumulants can also be expressed as polynomials in the central moments $\langle(\delta N)^n\rangle$, where $\delta N = N - \langle N\rangle$. The n-th moment $\langle N^n\rangle$ is linked to the net charge probability distribution through

$$\langle N^n\rangle = \sum_{N=-\infty}^{\infty} N^n P(N). \tag{2}$$

Cumulants of the net charge can exhibit singular properties near a phase transition. Consequently, it is interesting to study the effect of critical fluctuations on the corresponding probability distributions.

The aim of this paper is to explore the qualitative features of the probability distribution for the net baryon number near the chiral phase transition. Hence, we do not attempt the ambitious task to compute the probability distribution in QCD or in a QCD-like effective model. Instead, we study the fluctuations within a more transparent framework, Landau theory of phase transitions. This approach does not provide a quantitative description of the probability distribution. Nevertheless, the

qualitative aspects of our results are expected to be of general validity.

II. FLUCTUATIONS IN THE LANDAU THEORY

In this work, we explore the influence of a second-order phase transition on the probability distribution of conserved charges within Landau theory of phase transitions.

In Landau theory, the effective potential density ω at a given temperature T and baryon chemical potential μ is a polynomial in the order parameter σ,

$$\omega(T,\mu;\sigma) = \omega_{\rm bg} + \frac{1}{2}a(T,\mu)\sigma^2 + \frac{1}{4}\sigma^4, \tag{3}$$

where $\omega_{\rm bg}$ is a non-singular background contribution. Because we focus on a regular second-order phase transition, far from a possible tri-critical point (TCP), we can truncate the polynomial in Eq. (3) after the fourth order term. In general, the effective quartic coupling can also depend on T and μ. However, near the critical line $a(T_c,\mu_c)=0$ and sufficiently far away from a TCP, such a dependence is irrelevant. Furthermore, at $\mu = 0$ we set the transition temperature to $T_c = 0.15$ GeV and parametrize the non-singular part of the Landau thermodynamic potential density by

$$\omega_{\rm bg}/T^4 = -2d\cosh(\mu/T). \tag{4}$$

For $d = \pi^4/30$, the characteristic energy scale of the chiral phase transition in QCD is reproduced. This choice of parameters is clearly not unique. However, since we are interested in qualitative results, the precise choice of parameter values does not influence our conclusions.

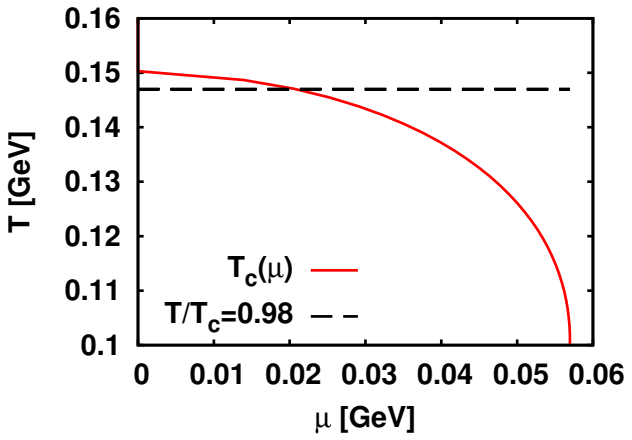

FIG. 1: The phase diagram of the Landau model for small chemical potentials. The horizontal line indicates the path along which the cumulants and probability distributions of charge fluctuations are calculated.

For positive $a(T,\mu)$, the minimum of the Landau potential (3) is located at $\sigma = 0$, while for $a(T,\mu) < 0$ the order parameter is non-zero, $\sigma = \pm\sqrt{-a(T,\mu)}$ and the symmetry is spontaneously broken. The parametrization of $a(T,\mu)$ is chosen so that the broken symmetry phase is located below the critical line $T = T_c(\mu)$, given by $a(T,\mu) = 0$. Consequently, the thermodynamic potential is

$$\omega_0 \equiv \omega(T > T_c(\mu),\mu) = \omega_{\rm bg}, \tag{5}$$

$$\omega_1 \equiv \omega(T < T_c(\mu),\mu) = \omega_{\rm bg} - \frac{1}{4}|a(T,\mu)|^2. \tag{6}$$

For the coefficient $a(T,\mu)$ we employ the following parameterization

$$a(T,\mu) = {\rm sign}\left[d(T,\mu)\right]\,|d(T,\mu)|^{1-\alpha/2}, \tag{7}$$

where

$$d(T,\mu) = -\left[3 - \frac{T}{T_c} - 2\cosh(\mu/T)\right]. \tag{8}$$

Note that for $\alpha = 0$, $a(T,\mu) = d(T,\mu)$. Moreover, for $|T-T_c|/T_c \ll 1$ and $\mu/T_c \ll 1$, Eq. (8) reduces to $d(T,\mu) \simeq A(T-T_c) + B\mu^2 \equiv t_\mu$, with $A > 0$ and $B > 0$. The scaling variable t_μ has been used frequently in the literature [4, 14].

The $\cosh(\mu/T)$ terms in Eqs. (4) and (8) account for the periodicity of the thermodynamic potential as a function of an imaginary baryon chemical potential, $\omega(T, i\theta T)$ with $\theta = \mu_I/T$ [28]. We note that this periodicity is identical to that of the QCD thermodynamic potential [29], when μ is the baryon chemical potential. We do not consider the confinement transition, and identify μ with the chemical potential of the elementary fermion.

The exponent α in Eq. (7) is introduced to parametrize the scaling properties of the thermodynamic potential. By tuning α, we can switch between $O(4)$ and mean-field scaling [1]. For $\alpha = 0$, the singular part of ω exhibits mean-field scaling. On the other hand, for the $O(4)$ value of the critical exponent of the specific heat, $\alpha \simeq -0.21$, the Landau potential emulates the critical behavior of the $O(4)$ spin system in 3-dimensions, when the critical line is approached from the broken phase [2].

In Fig. 1 we show the critical line $T_c(\mu_c)$ of the second order transition obtained in the Landau theory, using the parametrization (7) and (8) . The dependence of the first four cumulants on the chemical potential μ along a line of constant temperature is illustrated in Fig. 2 for $T/T_c = 0.98$.

Close to the critical point, at vanishing net baryon density ($|T-T_c|/T_c \ll 1$ and $\mu/T_c \ll 1$), the singular part

[1] This admittedly *ad hoc* procedure provides a transparent framework for exploring the effect of critical scaling on the cumulants of the net baryon number.

[2] Since other critical exponents are not reproduced, this statement is limited to quantities governed by the critical exponent α.

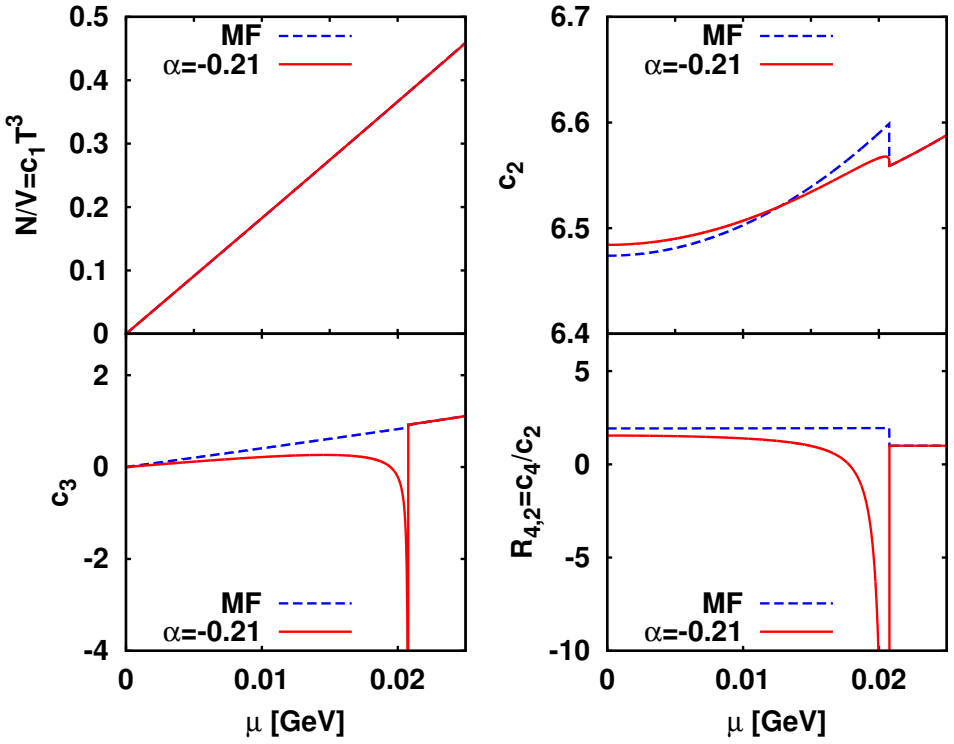

FIG. 2: The baryon number density N/V and the first three cumulants c_n obtained from the Landau potential Eqs. (5) and (6) for $T/T_c = 0.98$. The dashed lines shows the mean-field (MF) results with $\alpha = 0$, while the full lines correspond to $O(4)$ scaling, with $\alpha = -0.21$.

of the thermodynamic potential (5) and (6) scales as

$$\omega_{\rm sing} = -\frac{1}{4}|t_\mu|^{2-\alpha}, \tag{9}$$

for $T < T_c$, while for $T > T_c$ the singular part vanishes. For $\mu \neq 0$, the leading singularity of a given cumulant of the net baryon number is then given by

$$c_n^{\rm sing} \sim -\mu^n |t_\mu|^{2-\alpha-n}. \tag{10}$$

Using the $O(4)$ value for the exponent $\alpha \simeq -0.21$, the cumulants $c_n(T_c, \mu_c)$ diverge at the critical point for $n \geq 3$, as seen in Fig. 2. Moreover, in the model, the cumulants $c_n(T, \mu)$ are in general discontinuous at the transition point.

With the mean-field critical exponent $\alpha = 0$, the singular parts of the cumulants remain finite near the critical point. Indeed, differentiating Eq. (9) for $\alpha = 0$, one finds that for $T < T_c$, the non-vanishing cumulants are given by

$$c_1^{\rm sing} = -B\mu|t_\mu|, \quad c_2^{\rm sing} = -B|t_\mu| + 2B^2\mu^2, \tag{11}$$

$$c_3^{\rm sing} = 6B^2\mu, \qquad c_4^{\rm sing} = 6B^2. \tag{12}$$

Consequently, also in a mean-field approach, the cumulants are in general discontinuous at the critical point, as seen in Fig. 2, but they remain finite on both sides of the transition.

The singular behavior of the cumulants shown in Fig. 2 must be reflected in the corresponding probability distribution $P(N)$ of the net baryon number. In the following, we compute the distributions $P(N)$ in the mean-field and $O(4)$ cases and explore the characteristic features, which are responsible for the critical behavior of the cumulants illustrated in Fig. 2.

III. THE PROBABILITY DISTRIBUTION OF THE NET BARYON NUMBER

Consider a sub-volume V of a grand canonical thermodynamic system of charged particles q and anti-particles $\bar{q}$ at a given temperature T and chemical potential μ. The latter is related to the conserved net charge $N = N_q - N_{\bar{q}}$. The normalized probability distribution $P(N)$ for finding a net charge N in the volume V is given in terms of the canonical $Z(T, V, N)$ and grand canonical $\mathcal{Z}(T, V, \mu)$ partition functions [30–32],

$$P(N; T, \mu, V) = \frac{Z(T, V, N)e^{\beta\mu N}}{\mathcal{Z}(T, V, \mu)}, \tag{13}$$

where $\beta = 1/T$.

The grand canonical and canonical partition functions are linked through the fugacity expansion,

$$\mathcal{Z}(T,V,\mu) = \sum_N \lambda^N Z(T,V,N), \tag{14}$$

where $\lambda = e^{\beta\mu}$ is the fugacity parameter.

As follows from Eq. (14), the canonical partition function $Z(T,V,N)$ is just the N-th order coefficient in the Laurent expansion of $\mathcal{Z}(T,V,\mu)$ about $\lambda = 0\,(\mu = -\infty)$. It follows that, given $\mathcal{Z}(T,V,\mu)$, the canonical partition function $Z(T,V,N)$ can be obtained using

$$Z(T,V,N) = \frac{1}{2\pi i}\oint_C d\lambda \frac{\mathcal{Z}(T,V,\mu)}{\lambda^{N+1}}, \tag{15}$$

where the integration contour C must lie in an annulus enclosing the origin in the complex λ-plane. Inside the annulus the integrand $\mathcal{Z}(T,V,\mu)$ must be analytic (see Fig. 3).

Taking C on the unit circle, $\lambda = e^{i\theta}$, one finds the well-known result [30, 33],

$$Z(T,V,N) = \frac{1}{2\pi}\int_0^{2\pi} d\theta e^{-i\theta N}\mathcal{Z}(T,V,i\,T\,\theta). \tag{16}$$

We note that Eq. (16) holds only when $\mathcal{Z}(T,V,\mu)$ is analytic on the unit circle. In general, the partition function in finite systems[3], e.g. in lattice QCD simulations in a finite volume [35–40], is an analytic function of μ. Hence, in this case the integral (15) is well defined and independent of the radius of the contour.

However, for the partition function $\mathcal{Z} = e^{-\beta V\omega}$, where ω is approximated by the thermodynamic potential density in the *thermodynamic limit*, (5)-(6), while V is finite, there are singularities in the complex μ plane, which must be properly accounted for. This approximate treatment is justified for $|N| \ll N^*$, where N^* is a characteristic of the partition function of a finite system in the Yang-Lee theory of phase transitions [4].

To determine N^* for a given system, a microscopic computation of the grand canonical partition function in a finite volume is needed. However, such a calculation cannot be carried out within the Landau model considered here. Consequently, in the following we assume that N^* is larger than the maximal N, needed in the numerical evaluation of the probability distribution $P(N)$. We shall discuss the properties of the canonical partition function in this approximation.

[3] In a finite system, the partition function has Yang-Lee zeroes at complex μ, which in the thermodynamic limit turn into cuts [44], with branch points at the critical point and at $|\mu| = \infty$.

[4] In the original work of C. N. Yang and T.D. Lee [41], N^* is the maximum number of classical particles that can be packed into the volume V. The Yang-Lee theory was later extended to a more general class of models.

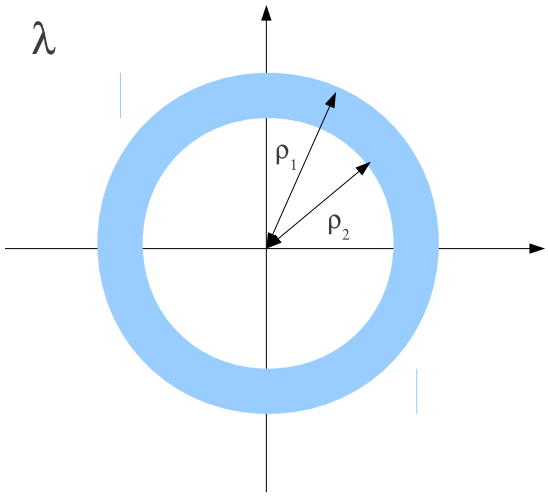

FIG. 3: The integration contour C in Eq. (15) lies within a singularity free annulus in the complex λ-plane, enclosing the origin.

In the chiral limit, a critical point exists on the positive real fugacity axis [42], $\lambda = \lambda_c > 1$. Charge conjugation symmetry of the partition function, $\mu \to -\mu$, implies that there is a corresponding critical point at $\lambda = 1/\lambda_c$. This symmetry is respected also by the thermodynamic potential (6).

At fixed temperature, the critical points at $\mu = \pm\mu_c$, or equivalently at $\lambda = \lambda_c^{\pm 1}$, are branch point singularities of the order parameter σ in the complex μ (or λ) plane [43], with the critical exponent β, $\sigma \sim (-t_\mu)^\beta$. In the mean-field approach, this singularity is of the square root type, i.e. $\beta = \frac{1}{2}$. Since in the mean-field approach $\omega_{\rm sing} \sim |a(T,\mu)|^2\,\theta(-a(T,\mu))$ and $a \sim t_\mu$, the singularity of the thermodynamic potential at the critical point is a discontinuity in the higher derivatives, i.e. in the cumulants c_n for $n \geq 2$, as shown in Fig. 2.

By contrast, for $\alpha = -0.21$, the critical points are branch points of the thermodynamic potential, $\omega_{\rm sing} \sim |t_\mu|^{2-\alpha}$. Consequently, the thermodynamic potential has cuts originating at the branch points. A convenient choice is to place the cuts on the real axis, between the critical point $\mu = \mu_c$ and $\mu = \infty$ as well as between $\mu = -\mu_c$ and $\mu = -\infty$. The corresponding cuts in the fugacity are located between $\lambda = \lambda_c > 1$ and $\lambda = \infty$ and between $\lambda = 1/\lambda_c$ and $\lambda = 0$, respectively [42]. As a result, in the thermodynamic limit, the thermodynamic potentials of different phases (in the present case, the ω_0 and ω_1) correspond to different Riemann surfaces connected through cuts [43].

If the grand canonical partition function $\mathcal{Z}$ exhibits branch singularities, then the coefficients of the Laurent expansion $Z(T,V,N)$, depend on the integration contour C in Eq. (15). In the broken-symmetry phase, the annulus is singularity free for $\rho_1 = \lambda_c > 1$ and $\rho_2 = 1/\lambda_c < 1$ (cf. Fig. 3). Thus, the coefficients of the Laurent expansion corresponding to the broken-symmetry phase, are

obtained using (16) with $\mathcal{Z} = e^{-\beta V\omega_1}$. On the other hand, the partition function $\mathcal{Z} = e^{-\beta V\omega_0}$ of the symmetric phase is singularity free outside the annulus of the broken symmetry phase. Hence, the corresponding Laurent coefficients are obtained by integrating (15) along e.g. a circular contour with radius $\rho < 1/\lambda_c$ or $\rho > \lambda$.

Thus, in general we obtain two competing partition functions for a given value of N. We note, however, that the partition function of a thermodynamic system must be unique. The reason for the ambiguity is the fact that we approximate ω in $\mathcal{Z}$ by the grand canonical thermodynamic potential density in the thermodynamic limit. In the limit $V \to \infty$, the uniqueness of the canonical partition function Z is restored, since the one corresponding to a larger value of ω is suppressed.

In this paper, we consider only the canonical partition function obtained from the grand canonical one using (15) for $\mu < \mu_c$, i.e. for the broken symmetry phase. The relation between the probability distribution $P(N)$ and the canonical partition function (13), implies that the structure of $P(N)$ is entirely governed by the properties of $Z(T, V, N)$.

The quantum statistics of fermion degrees of freedom, implies the existence of additional singularities in the complex μ plane, owing to the poles of the Fermi-Dirac distribution function [42]. The location of the "thermal" singularities may influence the possible choices of integration contour in Eq. (15), in particular for small values of the fermion mass. In the present model, which effectively corresponds to a Maxwell-Boltzmann treatment of the fermion degrees of freedom, these singularities are not accounted for.

A. Probability distribution of the nonsingular potential

The probability distribution corresponding to the nonsingular part of the thermodynamic potential ω_0 can be computed analytically. Indeed, using the generating function of the modified Bessel function $I_n(x)$,

$$e^{\frac{x}{2}(\lambda+\frac{1}{\lambda})} = \sum_{n=-\infty}^{\infty} I_n(x)\lambda^n, \tag{17}$$

one can directly expand the grand canonical partition function $\mathcal{Z} = e^{-\beta V\omega_0}$, without passing through the integral representation (15), and obtain [30, 34]

$$Z_0(T, V, N) = I_N(2dVT^3). \tag{18}$$

Here we used (4) and $\cosh(\mu/T) = (\lambda + 1/\lambda)/2$.

The probability distribution from the nonsingular part of the Landau potential (5) is then obtained from Eq. (13) as

$$P^{\rm NS}(N; T, V, \mu) = I_N(2dVT^3)e^{(\mu N+\Omega_0)/T}, \tag{19}$$

where $\Omega_0 = V\omega_0 = -2dVT^4\cosh(\mu/T)$ is the corresponding grand canonical potential.

B. Probability distribution of the mean-field potential

For the Landau potential (6) with the mean-field value for the exponent $\alpha = 0$, the canonical partition function $Z(T, V, N)$ may also be obtained analytically, using the same procedure as for the non-singular part.

The partition function of the singular case is written in the following from

$$e^{-\beta\Omega_1} = \exp\left\{VT^3\left[d\left(\lambda+\frac{1}{\lambda}\right)+\frac{1}{4}a^2(T,\mu)\right]\right\}. \tag{20}$$

By expanding the argument of the exponential (here we put $t = 1 - T/T_c$)

$$|a(T,\mu)|^2 = (t+2)^2 + 2 - 2(t+2)\left(\lambda+\frac{1}{\lambda}\right) + \lambda^2 + \frac{1}{\lambda^2}, \tag{21}$$

and using Eqs. (17) and (16), we find

$$Z_c^{\rm MF}(T, V, N) = e^{\frac{VT^3}{4}[(t+2)^2+2]} \times \sum_{\ell=-\infty}^{\infty} I_{N-2\ell}[(2d-t-2)VT^3]I_\ell\left(\frac{VT^3}{2}\right). \tag{22}$$

The probability distribution $P^{\rm MF}(N)$ can be then computed using Eqs. (20), (22) and (13),

$$P^{\rm MF}(N; T, V, \mu) = e^{VT^3\left(\frac{t+2}{2}-d\right)\left(\lambda+\frac{1}{\lambda}\right)-\frac{1}{4}\left(\lambda^2+\frac{1}{\lambda^2}\right)^2+\frac{\mu N}{T}} \times \sum_{\ell=-\infty}^{\infty} I_{N-2\ell}[(2d-t-2)VT^3]I_\ell\left(\frac{VT^3}{2}\right). \tag{23}$$

In Fig. 4 we show the resulting probability distributions $P^{\rm MF}(N)$ and $P^{\rm NS}(N)$ at $\mu = 0$ for $V = 30$ fm^3.

The mean-field probability distribution $P^{\rm MF}(N)$ is clearly broader than $P^{\rm NS}(N)$. This feature is also evident in the ratio $P^{\rm MF}(N)/P^{\rm NS}(N)$, shown in the right panel of Fig. 4. However, for small N, $|N| < 30$, the trend is reversed and $P^{\rm MF}$ is narrower than $P^{\rm NS}(N)$.

C. Probability distribution in the critical case

We have shown, that for the regular as well as singular part of the potential with the mean-field exponent $\alpha = 0$, the net charge probability distributions can be obtained in closed form. The singular part with $\alpha = -0.21$, however, does not allow for an analytic calculations. In this case, we can apply a numerical or some approximate analytical method to obtain the canonical partition function and the corresponding probability distribution $P^\alpha(N)$. The most direct approach to compute $Z(T, V, N)$, is the numerical integration of Eq. (16). There are, however, limitations of this method, in particular at large N, due to the oscillatory structure of the integrand. We adopt

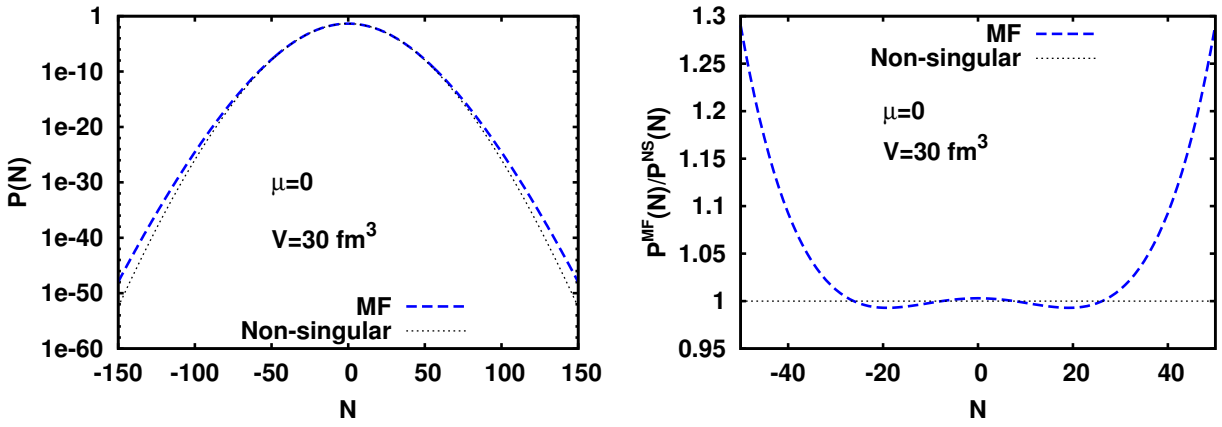

FIG. 4: Left : Probability distributions of the net baryon number in the Landau model. The left-hand figure shows the singular contribution in the mean-field case $P^{\rm MF}(N)$ from Eq. (23) (dashed-line) and the nonsingular $P^{\rm NS}(N)$ from Eq. (19) (dotted-line). The right-hand figure shows the ratio of these probability distributions. The calculations were done at $\mu = 0$ and for sub-volume $V = 30$ fm^3.

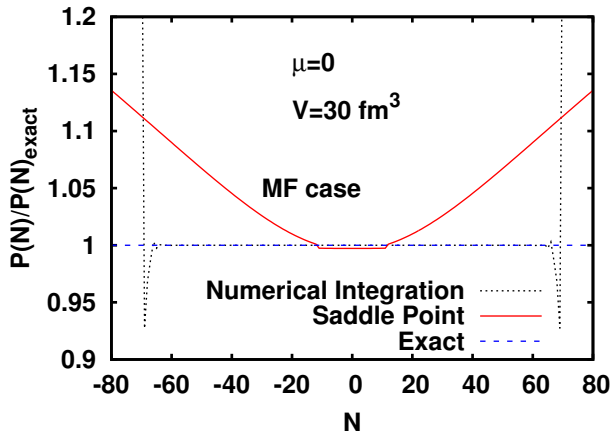

FIG. 5: Comparison of the probability distributions of the net baryon number $P(N)$ in the Landau model with the mean-field exponent calculated through different methods, see text. Each $P(N)$ is normalized to an exact result $P^{\rm MF}(N)$ from Eq. (23).

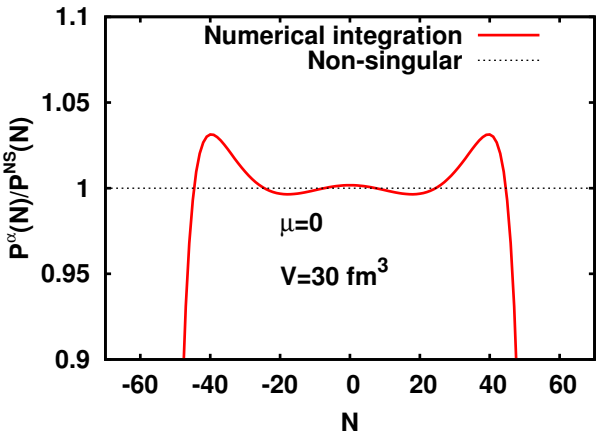

FIG. 6: The probability distribution calculated by the numerical integration from Eq. (16) in Landau model with $\alpha = -0.21$ and normalized to the non-singular probability distribution $P^{\rm NS}(N)$ from Eq. (19).

the `qawo` subroutine in QUADPACK package library for computing oscillatory integrals.

To test the numerical method, we first compare the probability distribution $P^{\rm MF}(N)$ obtained analytically in Eq. (23) with the numerical integration of Eq. (16). In Fig. 5 we show the ratio of the resulting probability distributions. The numerical integration reproduces the analytical result up to $|N| \simeq 60$, but fails for larger N. Thus, we conclude that the numerical integration can be used with confidence also to compute $P^{\alpha}(N)$ for the model with $\alpha \simeq -0.21$ up to this value of N.

In Fig. 6 we show the probability distribution $P^{\alpha}(N)$ obtained through numerical integration of Eq. (16), normalized to the non-singular distribution $P^{\rm NS}(N)$, Eq. (23). This ratio exhibits quite different behavior from that seen in Fig. 4 for the mean-field model. While $P^{\rm MF}(N)$ keeps increasing compared to $P^{\rm NS}(N)$, the singular distribution $P^{\alpha}(N)$ decreases relative to the non-singular background for large N. This indicates, that for the critical exponent $\alpha \simeq -0.21$, the singular probability distributions is narrower than the non-singular reference distribution.

The canonical partition function $Z(T, V, N)$ can also be computed by applying the method of steepest descent to the integral in Eq. (15). To this end, it is convenient to change the integration from the complex λ- to the complex μ-plane. The integration along the closed contour C, characterized by $\rho_2 < |\lambda| < \rho_1$ (see Fig. 3), is transformed into a line integral from $\mu = \mu_R - i\pi T$ to $\mu = \mu_R + i\pi T$, where μ_R is restricted to the range $-\mu_c < \mu_R < \mu_c$ (see Fig. 7). The canonical partition

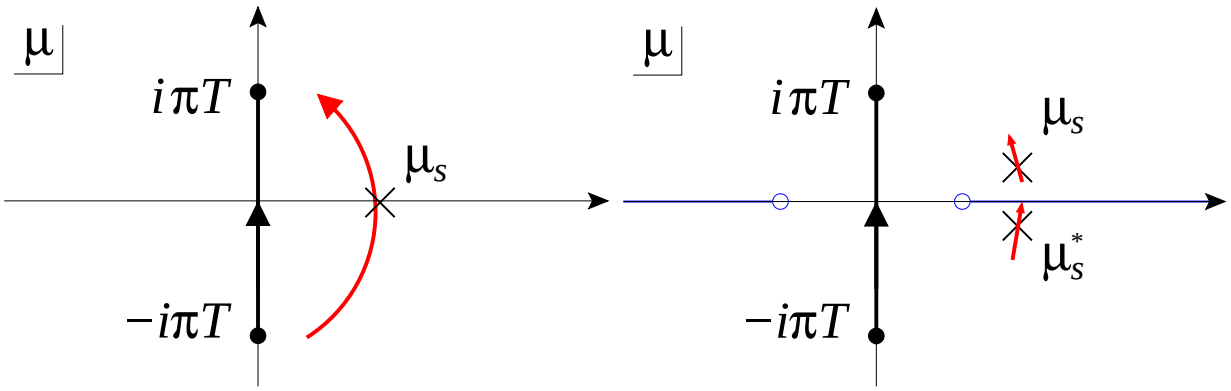

FIG. 7: The integration paths in the complex μ-plane of the integral (24). The left-hand figure, shows the path in the (MF) case where $\alpha = 0$ in (24). The solid line along the vertical axis denotes the original integration line and the shifted solid curve is the steepest descent path for the saddle point μ_s on the real μ axis. The right hand figure, shows the path for $\alpha = -0.21$ in (24). The lines on the horizontal axis, starting from $\mu = \pm\mu_c$ to $\pm\infty$, are the cuts of the integrand. The saddle points for $|N| > N_c$ are indicated by the crosses. The steepest descent path at the saddle point is indicated by the arrow.

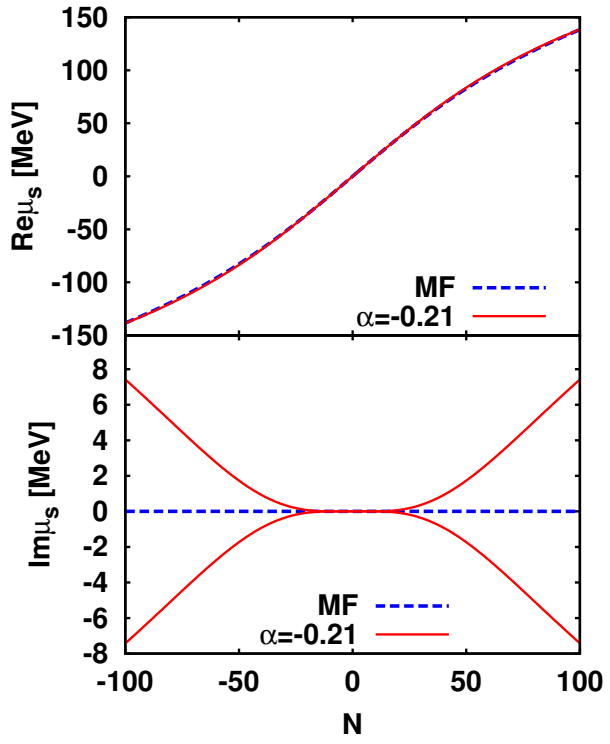

FIG. 8: The real part (top) and imaginary part (bottom) of the saddle point μ_s in the complex μ-plain as a function of N for the mean-field and the critical case with $\alpha = -0.21$.

function is then given by

$$Z(T,V,N) = \frac{\beta}{2\pi i}\int_{C_\mu} d\mu e^{VT^3 f(\mu)}, \qquad (24)$$

where

$$\begin{aligned} f(\mu) &= -\left(\omega_1(T,\mu) + \mu\, N/V\right)/T^4 \\ &= 2d\cosh(\mu/T) + \frac{1}{4}|a|^2(T,\mu) - \frac{\mu\, N}{VT^4}. \end{aligned} \qquad (25)$$

For sufficiently large values of the pre-factor VT^3, the integration (24) can be evaluated using the saddle-point approximation. For $V = 30$ fm^3 and $T = 150$ MeV, one finds $VT^3 \simeq 13$. This is reasonably large, so that we expect acceptable results in the saddle point approximation.

Let $\mu_s = \mu_s(T,V,N)$ be the solution of the saddle point condition

$$\left.\frac{\partial f(\mu)}{\partial \mu}\right|_{\mu_s} = 0. \qquad (26)$$

Then, the canonical partition function reads

$$Z(T,V,N) = \frac{1}{\sqrt{2\pi VT^5|f''(\mu_s)|}} e^{VT^3 f(\mu_s)}. \qquad (27)$$

Equation (25), implies that the saddle point condition (26) is given by

$$N = -\left(\frac{\partial \Omega}{\partial \mu}\right)_{T,V}; \qquad (28)$$

the thermodynamic relation for the average baryon number $N = \langle N\rangle$ in the grand canonical ensemble. For $\mu < \mu_c$ the relevant thermodynamic potential is that of the ordered phase, $\Omega = \Omega_1$. Thus, for $N < N_c$, where $N_c \sim 11$ is defined by the baryon number at the transition point $\mu = \mu_c$, the location of the saddle point μ_s is given by the density, shown in Fig. 2. On the other hand, for $N > N_c$ the saddle point condition is modified, as discussed below.

In the mean-field parametrization we find that the saddle point on the Ω_1 Riemann sheet is always located on the real axis, reflecting the lack of branch point singularities of the thermodynamic potential (see Fig. 7). On the other hand, in the critical case μ_s is real for $N < N_c$, but for $N > N_c$ there are two complex conjugate saddle points on either side of the cut, as shown in Fig. 7. The

imaginary part of the saddle points μ_s as a function of N is shown in Fig. 8 in the mean-field and in the critical case.

To test the validity, and the range of applicability of the saddle point method, we apply this approach to compute the canonical partition function and the corresponding probability distribution for the mean-field model. In Fig. 5 we show a comparison of $P(N)$ calculated using the saddle point integration with the analytical result $P^{\rm MF}(N)$, Eq. (23). The accuracy of the saddle point integration decreases with increasing $|N|$. With the parameters used in our calculations, the saddle point approximation reproduces $P^{\rm MF}(N)$ with sufficient accuracy, only for $|N| < 20$. The range of applicability in N is much smaller than that of direct numerical integration. We have verified, that by increasing VT^3, the range of applicability of the saddle-point approximation grows to larger $|N|$.

We note that the probability distribution $P^{\alpha}(N)$ obtained with the saddle point method exhibits larger deviations from the numerical results than in the mean-field case. The main problem is that in this case, for $N > N_c$ there are two complex conjugate saddle points, located close to the cut, as illustrated in Fig. 8. Consequently, there is also, in general a contribution to the integral emanating from the cut, which is neglected in the saddle point approximation.

Neglecting the cut and summing up the contributions from the two saddle points, the resulting partition function (24) reads,

$$Z(T,V,N) \simeq \frac{2}{\sqrt{2\pi VT^5|f''(\mu_s)|}} e^{VT^3 {\rm Re}[f(\mu_s)]} \times \cos(VT^3 {\rm Im}[f(\mu_s)]). \quad (29)$$

The $\cos(x)$ term in the above expression yields an oscillatory contribution to $P(N)$. This implies, that in some range of parameters, $P(N)$ is negative. This indicates, that the saddle point approximation in the present form has a rather restricted range of applicability.

In general, the appearance of the oscillatory factor in $P(N)$ is attributed to the contribution of the complex saddle points, resulting from the non-analyticity of the thermodynamic potential due to a phase transition. It is expected that in the physical case, this problem would be removed when the contribution of the cut is included.

In the present case, however, the onset of negative probabilities cannot be attributed solely to the complex structure of the saddle points. In fact, in our model, the negative probability appears for $|N| > 50$ also when the canonical partition function is evaluated numerically. Thus, the unphysical behavior of the canonical partition function seen in Eq. (29) might not only be attributed to the saddle point approximation but possibly also to an artefact of our model for the grand canonical partition function.

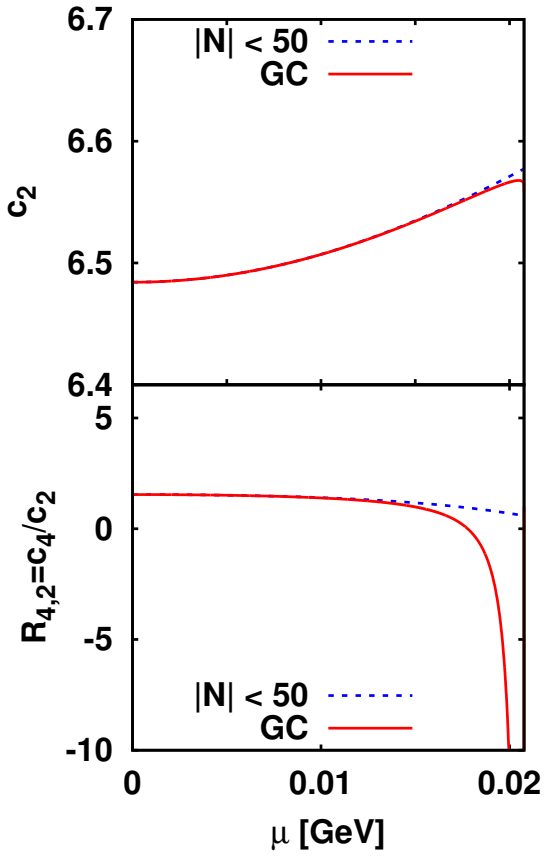

FIG. 9: Cumulants calculated from the probability distribution $P^{\alpha}(N)$ in Landau model for $\alpha = -0.21$. The $P^{\alpha}(N)$ was calculated numerically up to $|N| = 50$. The curve labelled GC is obtained directly from the grand canonical partition function using Eq. (1).

D. Cumulants calculated from $P(N)$

In the preceding section we have derived the probability distributions for the Landau potential applying two different methods, the numerical integration and the saddle point approximation. In general, the probability distribution exhibits characteristic structures near the phase transition, which are reflected in the critical behaviour of the cumulants. To explore the role of the critical fluctuations, we compute the cumulants directly from the probability distributions $P(N)$,

$$c_2(T,\mu) = \frac{1}{VT^3}\langle(\delta N)^2\rangle, \quad (30)$$

$$c_3(T,\mu) = \frac{1}{VT^3}\langle(\delta N)^3\rangle, \quad (31)$$

$$c_4(T,\mu) = \frac{1}{VT^3}\left[\langle(\delta N)^4\rangle - 3\langle(\delta N)^2\rangle^2\right], \quad (32)$$

where the average $\langle(\delta N)^n\rangle$ is defined in Eq. (2).

The analytic form of the mean-field probability distribution $P^{\rm MF}(N)$, reproduces the properties of cumulants shown in Fig. 2. The approximate $P^{\rm MF}(N)$ obtained

by numerical integration, yields cumulants c_n, which are consistent with exact results except for the immediate neighbourhood of the phase transition. Furthermore, the error of the saddle point approximation is at the few percent level for small μ, but increases as μ_c is approached. Such differences are expected, since the numerical and saddle point probability distributions do not reproduce the analytic results at large N.

In the model with the $O(4)$ critical exponent $\alpha = -0.21$, deviations are more pronounced. This is illustrated in Fig. 9, where the second- and the fourth-order cumulant, obtained using Eqs. (30)-(32) with $|N| < 50$ and the probability distribution evaluated numerically, are confronted with the exact results, computed using Eq. (1) with $p = -\omega_1$. The second order cumulant, which remains finite at the $O(4)$ critical point, is well reproduced, while the for fourth order cumulant, which diverges at the transition point at finite density, we find agreement only at small $\mu < \mu_c$. Thus, the approximate cumulant completely fails to reproduce the critical structure near μ_c. This is closely related to the fact, that the $P(N)$ obtained by numerical integration does not reproduce the large N behaviour, as illustrated in Fig. 5 for the mean-field model. Since the fugacity factor $e^{\mu N/T}$ in Eq. (13) enhances the large N part of $P(N)$ for $\mu > 0$, $P(N)$ at $|N| > 50$, which is negligible in $P(N)$ at $\mu \ll \mu_c$, becomes necessary to reproduce the higher order cumulant.

Moreover, in our calculation the sub-volume is rather small and therefore the critical structure of the higher-order cumulants at the second order transition is not clearly exhibited. In order to reproduce the singular structure at the critical point in the cumulants of $P(N)$, the probability distribution in a larger sub-volume and at large N is needed [45]. Owing to the oscillatory behaviour of the integrand, the methods presented here, numerical integration or the saddle point approximation, do not provide access to this parameter range. The oscillatory integrand causes problems with the numerical integration of Eq. (15) while the rather complicated analytic structure of the grand canonical partition function at complex μ interferes with the saddle point approximation.

IV. CONCLUSIONS

We have explored the properties of the probability distributions $P(N)$ of the net baryon number in systems that exhibit a second order chiral phase transition. The critical behavior was modelled within the Landau theory of phase transitions, where the effective thermodynamic potential is expressed as a polynomial in the order parameter. The coefficients of the effective potential were parametrized such that the scaling behavior of the specific heat and of the cumulants of the net baryon number in the mean-field approach and in the $O(4)$ universality class, respectively, is reproduced. The resulting effective potential preserves the baryon-anti baryon symmetry and the periodicity in the imaginary baryon-chemical potential, obtained in QCD.

In the mean-field approach, where the specific heat critical exponent $\alpha = 0$, the probability distribution of the net baryon number was computed analytically. In the model which reproduces the $O(4)$ scaling of the net charge fluctuations, the probability distribution could not be obtained in closed form. In this case we applied the numerical and the saddle point methods to calculate $P(N)$ and we discussed the validity and the limitations of these methods.

We have shown that in the mean-field case, the contribution of the singular part of the thermodynamic potential, which is responsible for the critical behaviour of the order parameter, results in a broadening of the probability distribution. On the other hand, in the model, which exhibits $O(4)$ scaling of the net baryon number fluctuations, the contribution of the singular part results in the opposite behaviour, i.e. in a narrower net baryon number probability distribution. However, using the numerically computed $O(4)$ probability distribution $P(N)$, we are not able to reproduce the critical behaviour of the net baryon number cumulants. The main reason for this failure is, that the resulting probability distribution $P(N)$ is applicable only up to a finite $|N| < 50$ and in a rather small volume. In order to reproduce the singular structure of higher-order cumulants directly from the probability distribution one would need to compute $P(N)$ for large net baryon number N and for a sufficiently large volume.

Acknowledgments

K.M. would like to thank RIKEN-BNL Research Center for their warm hospitality during his visit where part of this work was completed. The authors also would like to thank P. de Forcrand, F. Karsch and A. Ohnishi for fruitful discussion. This work was in part supported by the young researchers exchange program by the Yukawa Institute for Theoretical Physics, by Yukawa International Program for Quark-Hadron Sciences at Kyoto University, and by the Grants-in-Aid for Scientific Research from JSPS No.24540271. K.R. acknowledges partial support of the Polish Ministry of National Education (MEN). The research of V.S. is supported under Contract No. DE-AC02-98CH10886 with the U. S. Department of Energy. B.F. is supported in part by the ExtreMe Matter Institute EMMI.

[1] M. Asakawa, U. W. Heinz and B. Muller, Phys. Rev. Lett. **85**, 2072 (2000); Nucl. Phys. **A698**, 519 (2002).

[2] S. Jeon and V. Koch, Phys. Rev. Lett. **85**, 2076 (2000);

V. Koch, M. Bleicher and S. Jeon, Nucl. Phys. **A698**, 261 (2002); V. Koch, J. Phys. G **35**, 104030 (2008).
[3] M. Stephanov, K. Rajagopal, and E. Shuryak, Phys. Rev. Lett. **81**, 4816 (1998); Phys. Rev. D **60**, 114028 (1999).
[4] S. Ejiri, F. Karsch and K. Redlich, Phys. Lett. B **633**, 275 (2006).
[5] F. Karsch and K. Redlich, Phys. Lett. B **695**, 136 (2011)
[6] Y. Hatta and M. A. Stephanov, Phys. Rev. Lett. **91**, 102003 (2003).
[7] M. Asakawa, and K. Yazaki, Nucl. Phys. **A504**, 668 (1989).
[8] M. A. Stephanov, Phys. Rev. Lett. **102**, 032301 (2009).
[9] M. A. Stephanov, Phys. Rev. Lett. **107**, 052301 (2011).
[10] P. Braun-Munzinger, B. Friman, F. Karsch, K. Redlich, and V. Skokov, Phys. Rev. C **84**, 064911 (2011); Nucl. Phys. **A880**, 48 (2012).
[11] V. Skokov, B. Friman, E. Nakano, K. Redlich, and B.-J. Schaefer, Phys. Rev. D **82**, 034029 (2010).
[12] V. Skokov, B. Friman, F. Karsch and K. Redlich, J. Phys. G **38**, 124102 (2011).
[13] B. Friman, F. Karsch, K. Redlich and V. Skokov, Eur. Phys. J. C **71**, 1694 (2011).
[14] V. Skokov, B. Friman, and K. Redlich, Phys. Rev. C **83**, 054904 (2011).
[15] R. D. Pisarski and F. Wilczek, Phys. Rev. D **29**, 338 (1984).
[16] S. Ejiri, F. Karsch, E. Laermann, C. Miao, S. Mukherjee, P. Petreczky, C. Schmidt, W. Soeldner, and W. Unger, Phys. Rev. D **80**, 094505 (2009).
[17] F. Karsch, E. Laermann, C. Miao, S. Mukherjee, P. Petreczky, C. Schmidt, W. Soeldner and W. Unger, Phys. Rev. D **83**, 014504 (2011).
[18] M. Kitazawa and M. Asakawa, Phys. Rev. C **85**, 021901 (2012).
[19] M. M. Aggarwal *et al.* [STAR Collaboration], Phys. Rev. Lett. **105**, 022302 (2010); X. Luo, *et al.*, [for the STAR Collaboration], J. Phys. Conf. Ser. **316** 012003 (2011).
[20] C.R. Allton, M. Döring, S. Ejiri, S.J. Hands, O. Kaczmarek, F. Karsch, E. Laermann and K. Redlich Phys. Rev. **D71**, 054508 (2005).
[21] A. Bazavov and P. Petreczky, J. Phys. Conf. Ser. **230** 012014 (2010).
[22] S. Borsanyi, Z. Fodor, C. Hoelbling, S. D. Katz, S. Krieg, C. Ratti and K. K. Szabo [Wuppertal-Budapest Collaboration], JHEP **1009**, 073 (2009).
[23] A. Bazavov *et al.* [HotQCD Collaboration], arXiv:1203.0784 [hep-lat].
[24] B. Stokic, B. Friman and K. Redlich, Phys. Lett. B **673**, 192 (2009); V. Skokov, B. Stokic, B. Friman and K. Redlich, Phys. Rev. C **82**, 015206 (2010).
[25] C. Sasaki, B. Friman and K. Redlich, J. Phys. G **35**, 104095 (2008); C. Sasaki, B. Friman and K. Redlich, Phys. Rev. D **75**, 074013 (2007); C. Sasaki, B. Friman and K. Redlich, Phys. Rev. D **75**, 054026 (2007);
[26] M. Asakawa, S. Ejiri and M. Kitazawa, Phys. Rev. Lett. **103**, 262301 (2009).
[27] T. K. Herbst, J. M. Pawlowski and B. -J. Schaefer, Acta. Phys. Pol. B (Proc. Suppl.) **5**, 733 (2012), [arXiv:1202.0758 [hep-ph]].
[28] K. Morita, V. Skokov, B. Friman and K. Redlich, Phys. Rev. D **84**, 076009 (2011); Phys. Rev. D **84**, 074020 (2011); Acta. Phys. Pol. B (Proc. Suppl.) **5**, 803 (2012)[arXiv:1111.3446 [hep-ph]].
[29] A. Roberge and N. Weiss, Nucl. Phys. **B275**, 734 (1986).
[30] P. Braun-Munzinger, K. Redlich, J. Stachel, in Quark-Gluon Plasma 3, Eds. R.C. Hwa and X.N. Wang, (World Scientific Publishing, 2004).
[31] J. Cleymans, P. Koch, Z. Phys. C **52**, 137 (1991);
C. M. Ko, V. Koch, Z.-W. Lin, K. Redlich, M. A. Stephanov, and X.-N. Wang, Phys. Rev. Lett. **86**, 5438 (2001).
[32] J. Cleymans, K. Redlich and L. Turko, Phys. Rev. C **71**, 047902 (2005).
[33] R. Hagedorn and K. Redlich, Z. Phys. C**27**, 541 (1985).
[34] P. Braun-Munzinger, J. Cleymans, H. Oeschler and K. Redlich, Nucl. Phys. **A697**, 902 (2002).
[35] M. Alford, A. Kapustin, and F. Wilczek, Phys. Rev. D **59**, 054502 (1999).
[36] P. de Forcrand and S. Kratochvila, Nucl. Phys. B. (Proc. Suppl.) **153**, 62 (2006).
[37] S. Ejiri, Phys. Rev. D **78**, 074507 (2008).
[38] A. Li, A. Alexandru, K. F. Liu, and X. Meng, Phys. Rev. D **82**, 054502 (2010).
[39] A. Li, A. Alexandru, and K.-F. Liu, Phys. Rev. D **84**, 071503(R) (2011).
[40] K. Nagata, S. Motoki, Y. Nakagawa, A. Nakamura, and T. Saito (XQCD-J Collaboration), Prog. Theor. Exp. Phys. 01A103 (2012) [arXiv:1204.1412 [hep-lat]].
[41] C. -N. Yang and T. D. Lee, Phys. Rev. **87**, 404 (1952).
[42] V. Skokov, K. Morita, and B. Friman, Phys. Rev. D **83**, 071502(R) (2011).
[43] B. Friman, Acta. Phys. Pol. B (Proc Suppl.) **5**, 707 (2012), arXiv:1202.0021 [hep-ph].
[44] M. Stephanov, Phys. Rev. D **73**, 094508 (2006).
[45] K. Morita *et al.* (in preparation)